Unwrapped phase inversion for near surface seismic data

Yunseok Choi and Tariq Alkhalifah, King Abdullah University of Science and Technology*

Summary

The Phase-wrapping is one of the main obstacles of waveform inversion. We use an inversion algorithm based on the instantaneous-traveltime that overcomes the phase-wrapping problem. With a high damping factor, the frequency-dependent instantaneous-traveltime inversion provides the stability of refraction tomography, with higher resolution results, and no arrival picking involved. We apply the instantaneous-traveltime inversion to the synthetic data generated by the elastic time-domain modeling. The synthetic data is a representative of the near surface seismic data. Although the inversion algorithm is based on the acoustic wave equation, the numerical examples show that the instantaneous-traveltime inversion generates a convergent velocity model, very similar to what we see from traveltime tomography.

Introduction

Although waveform inversion can generate a precise velocity model, it suffers from the infamous local minima problem. A major reason for the local minima problem is the wrapping around nature of phase in the frequency domain or the cycle skipping that takes place in the time domain (Bunks et al., 1995; Virieux and Operto, 2009). Since the phase of the Fourier transformed wavefield has a finite but periodic range $[0, 2\pi]$, the modeled phase could converge to the wrong phase corresponding to a different cycle in the procedure of waveform inversion, which makes the inversion converge to a local minimum.

To overcome the phase wrapping problem, Shin et al. (2003) used the derivative wavefield with respect to the angular frequency. Taking the derivative of the wavefield with respect to the angular frequency makes the phase information appear in the amplitude component as well. Because the amplitude component is not limited in range, getting the phase information from the amplitude component overcomes the phase-wrapping problem even at high frequencies. Shin et al. (2003) used this algorithm to calculate the first arrival traveltime from the forward-modeled wavefield in the frequency-domain.

Recently, Choi and Alkhalifah (2011) have developed an inversion algorithm using the instantaneous-traveltime (with unwrapped phase features). The instantaneous-traveltime is obtained by dividing the derivative wavefield with respect to the angular frequency by wavefield itself and taking its imaginary part. Choi and Alkhalifah (2011) constructed the objective function using the instantaneous-traveltime and derived the gradient of the objective

function using the back-propagation algorithm based on the adjoint-state technique (Laily, 1983; Tarantola, 1984; Gauthier et al., 1986; Choi et al., 2008a,b).

Inversion relies very much on large offsets and shallow refraction type events for information. These ingredients are at the heart of what we need for near surface velocity estimation. However, data recorded from the near surface typically have elastic nature of the subsurface more evident than those corresponding to deeper events, which poses a challenge to the classical acoustic medium waveform inversion. The main objective of this abstract is to apply the instantaneous-traveltime inversion based on the acoustic wave equation to the near-surface seismic data. To validate the feasibility of the instantaneous-traveltime inversion to the near-surface seismic data, we first generate the synthetic data for shallow depth model using the elastic time-domain modeling technique and apply the instantaneous-traveltime inversion to the synthetic data. In this application, we use a strong damping factor. With a strong damping factor, the instantaneous-traveltime inversion becomes more similar to the wave-based refraction tomography (Min and Shin, 2006).

However, compared to refraction tomography, the instantaneous-traveltime inversion does not require traveltime picking. We can estimate the instantaneous-traveltime automatically from the Fourier-transformed recorded-data. Since we use a strong damping factor, the estimated instantaneous-traveltime from the elastic time-domain modeled data is almost the same as that from the acoustic modeled data. Therefore, with a strong damping, the instantaneous-traveltime inversion based on the acoustic wave-equation can be applied even to the elastic time-domain modeled data without traveltime picking.

In the following section, we start by introducing the instantaneous-traveltime inversion algorithm. Next, we will show numerical examples of inversion on synthetic data.

Instantaneous traveltime and its inversion algorithm

First, we revisit the concept of instantaneous-traveltime (or unwrapped phase) corresponding to a wavefield. Then, we introduce an inversion algorithm using the instantaneous-traveltime (Choi and Alkhalifah, 2011).

We assume that a seismic signal can be approximated by a series of weighted spikes (Shin et al., 2002):

$$u(t) = \sum_n A_n \delta(t - t_n), \qquad (1)$$

where A_n is the amplitude for the n-th digitized time, t_n. If we multiply equation 1 by a strong damping factor $e^{-\alpha t}$, we can suppress all the events following the first arrival and thus approximate the solution as

$$u^*(t) = u(t)e^{-\alpha t} \cong A_1 e^{-\alpha t}\delta(t - t_1), \qquad (2)$$

where A_1 and t_1 are the amplitude and the traveltime of the first arrival event. Equation 2 can be written in the frequency-domain as

$$\hat{u}(\omega) = \tilde{A}e^{-i\omega t_1}, \qquad (3)$$

where $\tilde{A} = A_1 e^{-\alpha t_1}$ and ω is the angular frequency. Taking the derivative of equation 3 with respect to the angular frequency gives

$$\frac{\partial \hat{u}(\omega)}{\partial \omega} = -it_1 \tilde{A}e^{-i\omega t_1} = -it_1 \hat{u}(\omega). \qquad (4)$$

From equation 4, we can compute the instantaneous-traveltime (or may be referred to as the unwrapped phase) by dividing the derivative wavefield by wavefield itself and taking the imaginary part as follows:

$$t_1(\omega) = \text{Im}\left(\frac{\partial \hat{u}(\omega)}{\partial \omega} \middle/ \hat{u}(\omega) \right). \qquad (5)$$

In equation 5, since the amplitude component is not limited in range, the traveltime t_1, which appears in the amplitude component, is not affected by the phase wrapping phenomenon.

We can calculate the derivative wavefield in equation 4 from the modeled wavefield using a virtual source (Choi and Alkhalifah, 2011). The frequency-domain (Helmholtz equation) modeling can be expressed in matrix form as follows

$$\mathbf{S}(\omega)\hat{\mathbf{u}}(\omega) = \mathbf{f}, \qquad (6)$$

where $\mathbf{S}$ is the impedance matrix, $\hat{\mathbf{u}}$ is the wavefield vector, and $\mathbf{f}$ is the source vector. Taking the derivative of equation 6 with respect to ω gives

$$\mathbf{S}(\omega)\frac{\partial \hat{\mathbf{u}}(\omega)}{\partial \omega} = -\frac{\partial \mathbf{S}(\omega)}{\partial \omega}\hat{\mathbf{u}}(\omega). \qquad (7)$$

The right-hand side of equation 7 is the virtual source. If we regard this as a new source vector, we can calculate the derivative of the wavefield ($\partial \hat{\mathbf{u}}(\omega)/\partial \omega$) through a new modeling procedure with the same operator $\mathbf{S}$.

The instantaneous-traveltime of the recorded-data is obtained in a different way from that of the modeled wavefield. A basic feature of Fourier transform is its capability in simplifying a derivative in the frequency domain by:

$$F\left[itd(t)\right] = \frac{\partial \hat{d}(\omega)}{\partial \omega}, \qquad (8)$$

where i is the imaginary unit and $d(t)$ is the recorded data. Thus, to obtain the derivative of the recorded data with respect to the angular frequency, we multiply the original signal with 'it' and take it's Fourier-transform. In this case the instantaneous-traveltime is given by dividing $F\left[itd(t)\right]$ by $i\hat{d}$.

The objective function for inversion is constructed using the instantaneous traveltime (Choi and Alkhalifah, 2011) as follows (for one shot gather and one frequency):

$$E = \sum_{j=1}^{nr}\left[\text{Im}\left\{ \left(\frac{\partial \hat{u}_j}{\partial \omega}\right) \middle/ \hat{u}_j \right\} - \text{Im}\left\{ \left(\frac{\partial \hat{d}_j}{\partial \omega}\right) \middle/ \hat{d}_j \right\} \right]^2, \qquad (9)$$

where $\hat{u}_j$ and $\hat{d}_j$ are the modeled and observed wavefields at the j-th receiver and 'Im' indicates the imaginary part. The gradient of equation 9 is obtained by taking the derivative of this equation with respect to the i-th model parameter p_i and expressed as

$$\frac{\partial E}{\partial p_i} = 2\sum_{j=1}^{nr}\text{Im}\left[\frac{\partial^2 \hat{u}_j}{\partial p_i \partial \omega}\frac{1}{\hat{u}_j}\text{Im}\left[\left(\frac{\partial \hat{u}_j}{\partial \omega}\right) \middle/ \hat{u}_j - \left(\frac{\partial \hat{d}_j}{\partial \omega}\right) \middle/ \hat{d}_j \right] \right] +$$
$$2\sum_{j=1}^{nr}\text{Im}\left[-\frac{\partial \hat{u}_j}{\partial p_i}\frac{\left(\partial \hat{u}_j/\partial \omega\right)}{\hat{u}_j^2}\text{Im}\left[\left(\frac{\partial \hat{u}_j}{\partial \omega}\right) \middle/ \hat{u}_j - \left(\frac{\partial \hat{d}_j}{\partial \omega}\right) \middle/ \hat{d}_j \right] \right] \qquad (10)$$

Consequently, the gradient of the objective function is expressed in matrix form based on the adjoint-state technique of wave equation as follows

$$\frac{\partial E}{\partial p_i} = 2\text{Im}\left[\left(-\frac{\partial \mathbf{S}}{\partial p_i}\frac{\partial \hat{\mathbf{u}}}{\partial \omega} - \frac{\partial^2 \mathbf{S}}{\partial p_i \partial \omega}\hat{\mathbf{u}} \right)^T \mathbf{S}^{-1}\mathbf{r}_1 + \right.$$
$$\left. \left(-\frac{\partial \mathbf{S}}{\partial p_i}\hat{\mathbf{u}} \right)^T \mathbf{S}^{-1}\left\{ \left(-\frac{\partial \mathbf{S}}{\partial \omega} \right)^T \mathbf{S}^{-1}\mathbf{r}_1 \right\} \right] - 2\text{Im}\left[\left(-\frac{\partial \mathbf{S}}{\partial p_i}\hat{\mathbf{u}} \right)^T \mathbf{S}^{-1}\mathbf{r}_2 \right] \qquad (11)$$

where the elements of $\mathbf{r}_1$ are written as

$$r_{1i} = \frac{1}{u_j}\text{Im}\left[\left(\frac{\partial \hat{u}_j}{\partial \omega}\right) \middle/ \hat{u}_j - \left(\frac{\partial \hat{d}_j}{\partial \omega}\right) \middle/ \hat{d}_j \right], \qquad (12)$$

and the elements of $\mathbf{r}_2$ are written as

$$r_{2i} = \frac{\left(\partial \hat{u}_j/\partial \omega\right)}{\hat{u}_j^2}\text{Im}\left[\left(\frac{\partial \hat{u}_j}{\partial \omega}\right) \middle/ \hat{u}_j - \left(\frac{\partial \hat{d}_j}{\partial \omega}\right) \middle/ \hat{d}_j \right]. \qquad (13)$$

In equation 11, to calculate the gradient, we back-propagate $\mathbf{r}_1$, $\mathbf{r}_2$, and $\left\{ \left(-\partial \mathbf{S}/\partial \omega\right)^T \mathbf{S}^{-1}\mathbf{r}_1 \right\}$, and multiply the back-propagated wavefield with virtual wavefields, $\left(-\frac{\partial \mathbf{S}}{\partial p_i}\frac{\partial \hat{\mathbf{u}}}{\partial \omega} - \frac{\partial^2 \mathbf{S}}{\partial p_i \partial \omega}\hat{\mathbf{u}} \right)^T$ and $\left(-\frac{\partial \mathbf{S}}{\partial p_i}\hat{\mathbf{u}} \right)^T$, respectively.

We use the steepest descent direction for optimization. We also use the conjugate-gradient approach (Gill et al., 1981) to find the optimum search direction for updating model

parameters. To obtain a proper step length, we could employ a line-search method, but, for simplicity, we fix the value of the step length.

Examples

We first generate the synthetic data using the elastic time-domain modeling technique for the modified SEG/EAGE overthrust model. We downsize the model and slightly modify the P- and S-wave velocities. The grid interval is 10 m and the model size is 6 Km horizontal range and 0.6 Km in the depth. We assume that the density is constant. We display the modified P-wave and S-wave velocity of the modified SEG/EAGE overthrust model in Figure 1. The recording time is 2.5 seconds and time-step for modeling is 1 ms. We place 141 shots with an interval of 40 m and place the receivers at all grid points. We ignite only a vertical direction source and record only the vertical component of displacement. The synthetic data set is representative of the near-surface land seismic data. Figure 2 shows a generated synthetic seismogram of the vertical displacement where the shot is located at the distance of 0.55 Km. We note that the Rayleigh wave is very dominant in the seismogram. Using equation 8, we estimate the instantaneous-traveltime with a high damping factor from the synthetic seismogram. Figure 3 shows the estimated instantaneous-traveltime from the seismogram in Figure 2. Because of the effect of source wavelet, the estimated instantaneous-traveltime is constantly shifted from the true onset value. We compensate for the shift by assuming that the source wavelet is known (Figure 3). The estimated traveltime also shows some severe fluctuations near the shot position, which results from the polarity changes of the first arrival events near the shot position. In the inversion, we exclude data where the offset distance is shorter than 0.3 Km.
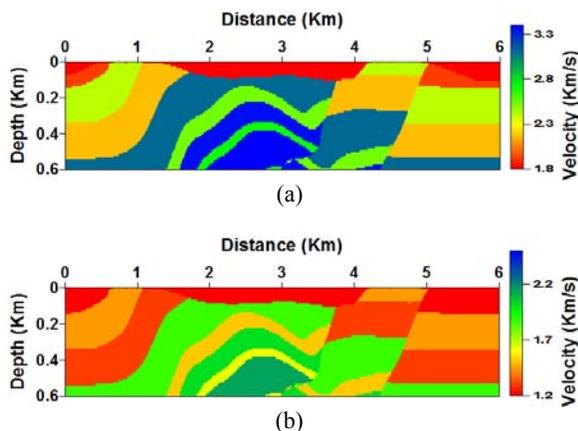

Figure 1. The (a) P-wave and (b) S-wave velocity of the modified SEG/EAGE overthrust model.
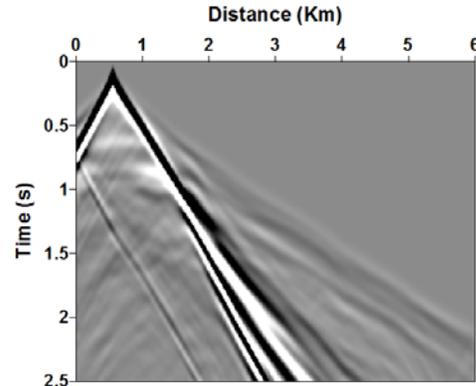

Figure 2. The synthetic seismogram of vertical displacement generated by the elastic time-domain modeling.
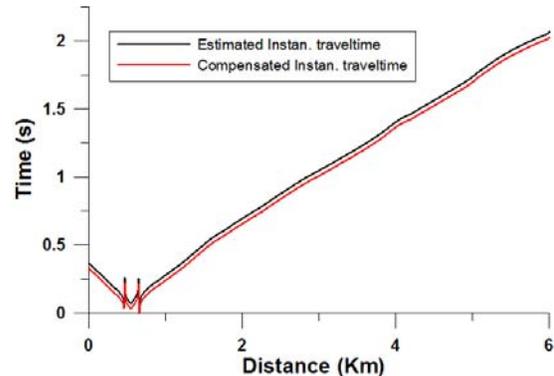

Figure 3. The estimated and compensated instantaneous-traveltime from the synthetic seismogram in Figure 2.

We apply the instantaneous-traveltime inversion algorithm to the synthetic data. We perform a single frequency inversion. The frequency and damping factor used for the single frequency inversion are 0.4 Hz and e^{-60t}. We ran 200 iterations for the inversion using the steepest-descent optimization approach. Figure 4 shows the starting model and the final inverted velocity model. We note that our inversion algorithm yields a smoothly recovered structure of the true model, which looks like a tomographic result. Figure 5 shows the history of the model fit between the true P-wave model and the inverted models, which demonstrate the inverted models converge smoothly to the right answer. Figure 6 shows the history of the misfit function of the instantaneous-traveltime. Figure 7 shows the observed instantaneous traveltime (compensated) and the modeled instantaneous traveltime for the starting model and inverted model. Figures 6 and 7 demonstrate the validity of our inversion algorithm.

Unwrapped phase inversion for near surface seismic data
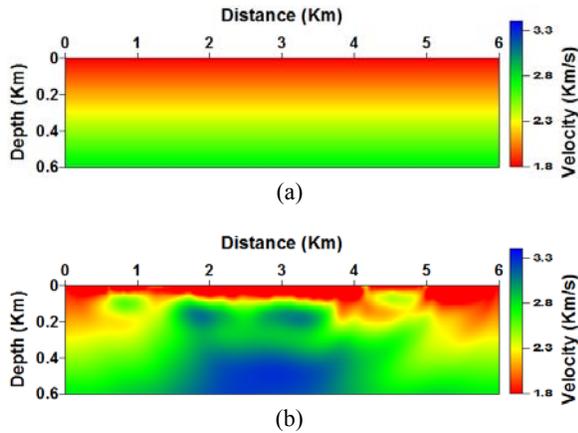

(a)

(b)

Figure 4. The (a) starting velocity model for the inversion and (b) final inverted velocity model after 200 iterations.
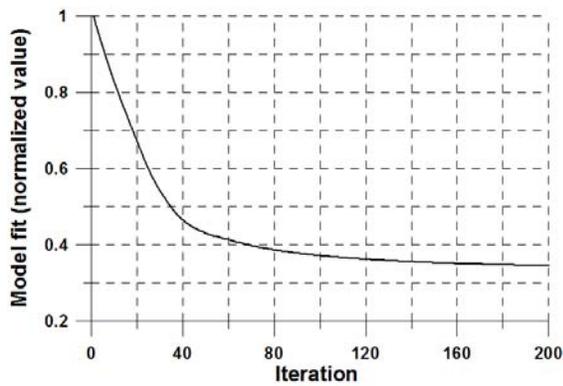

Figure 5. The history of the model fit between the true model and the inverted model at each iteration.
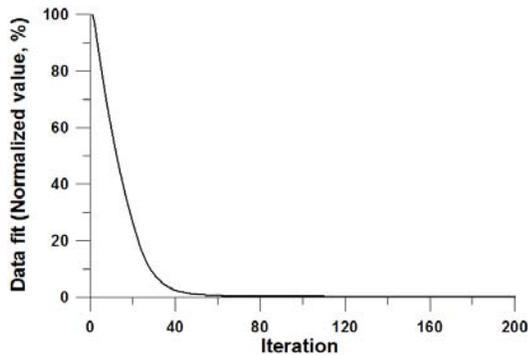

Figure 6. The history of the misfit function for the instantaneous-traveltime inversion.
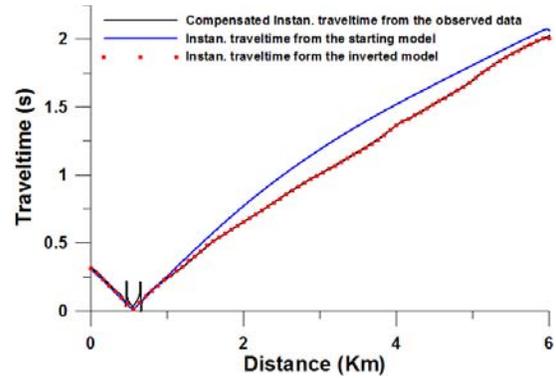

Figure 7. The observed instantaneous-traveltime (compensated) and the modeled instantaneous-traveltime using the frequency-domain modeling approach for the starting model and final inverted model.

Conclusions

Since the instantaneous-traveltime does not suffer from phase wrapping, the inversion algorithm using the instantaneous-traveltime has the potential to generate robust inversion results. With a high damping factor, the instantaneous-traveltime inversion provides refraction tomography similar results, but from a single frequency, and without the need to pick traveltimes. We apply the instantaneous-traveltime inversion with a high damping factor to the synthetic data generated using an elastic time-domain modeling. The synthetic data set is representative of the near surface seismic data. Although the inversion algorithm is based on the acoustic wave equation, the numerical examples show that our inversion algorithm generates a convergent smooth velocity model, which looks very much like a tomographic result. Next, we plan to apply the instantaneous-traveltime inversion algorithm on real seismic data acquired from the near surface.

Acknowledgments

EDITED REFERENCES

Note: This reference list is a copy-edited version of the reference list submitted by the author. Reference lists for the 2012 SEG Technical Program Expanded Abstracts have been copy edited so that references provided with the online metadata for each paper will achieve a high degree of linking to cited sources that appear on the Web.

REFERENCES

Bunks, C., F. M. Saleck, S. Zaleski, and G. Chavent, 1995, Multiscale seismic waveform inversion: Geophysics, **60**, 1457-1473.

Choi, Y., and T. Alkhalifah, 2011, Frequency-domain waveform inversion using the unwrapped phase: 81st Annual International Meeting, SEG, Expanded Abstracts, 2576-2580.

Choi, Y., D. J. Min, and C. Shin, 2008a, Frequency-domain full waveform inversion using the new pseudo-Hessian matrix: Experience of elastic Marmousi-2 synthetic data: Bulletin of the Seismological Society of America, **98**, 2402-2415.

Choi, Y., D. J. Min, and C. Shin, 2008b, Two-dimensional waveform inversion of multi-component data in acoustic-elastic coupled media: Geophysical Prospecting, **56**, 863-881.

Gauthier, O., J. Virieux, and A. Tarantola, 1986, Two-dimensional nonlinear inversion of seismic waveforms: Numerical results: Geophysics, **51**, 1387-1403.

Gill, P. E., W. Murray, and M. Wright, 1981, Practical optimization: Academic Press, Inc.

Lailly, P., 1983, The seismic inverse problem as a sequence of before stack migration, *in* J. B. Bednar, R. Rednar, E. Robinson, and A. Weglein, eds., Conference on inverse scattering: Theory and application: SIAM.

Min, D. J., and C. Shin, 2006, Refraction tomography using a waveform-inversion back-propagation technique: Geophysics, **71**, no. 3, R21-R30.

Shin, C., S. Ko, W. Kim, D. J. Min, D. Yang, K. J. Marfurt, S. Shin, K. Yoon, and C. H. Yoon, 2003, Traveltime calculations from frequency-domain downward-continuation algorithms: Geophysics, **68**, 1380-1388.

Shin, C., D. J. Min, K. J. Marfurt, H. Y. Lim, D. Yang, Y. Cha, S. Ko, K. Yoon, T. Ha, and S. Hong, 2002, Traveltime and amplitude calculations using the damped wave solution: Geophysics, **67**, 1637-1647.

Tarantola, A., 1984, Inversion of seismic reflection data in the acoustic approximation: Geophysics, **49**, 1259-1266.

Virieux, J., and S. Operto, 2009, An overview of full-waveform inversion in exploration geophysics: Geophysics, **74**, no. 6, WCC1-WCC26.